

# A parametric level-set approach for topology optimization of flow domains

Georg Pingen · Matthias Waidmann ·  
Anton Evgrafov · Kurt Maute

Received: 4 December 2008 / Revised: 28 April 2009 / Accepted: 13 May 2009  
© Springer-Verlag 2009

**Abstract** Traditional methods based on an element-wise parameterization of the material distribution applied to the topology optimization of fluidic systems often suffer from slow convergence of the optimization process, as well as robustness issues at increased Reynolds numbers. The local influence of the design variables in the traditional approaches is seen as a possible cause for the slow convergence. Non-smooth material distributions are suspected to trigger premature onset of instationary flows which cannot be treated by steady-state flow models. In the present work, we study whether the convergence and the versatility of topology optimization methods for fluidic systems can be improved by employing a parametric level-set description. In general, level-set methods allow controlling the smoothness of boundaries, yield a non-local influence of design variables, and decouple the material description from the flow field discretization. The parametric level-set method used in this study uti-

lizes a material distribution approach to represent flow boundaries, resulting in a non-trivial mapping between design variables and local material properties. Using a hydrodynamic lattice Boltzmann method, we study the performance of our level-set approach in comparison to a traditional material distribution approach. By numerical examples, the parametric level-set approach is validated through comparison with traditional material distribution based methods. While the parametric level-set approach leads to similar optimal designs, the present study reveals no general improvements of the convergence of the optimization process and of the robustness of the nonlinear flow analyses when compared to the traditional material distribution approach. Instead, our numerical experiment suggests that a continuation method operating on the volume constraint is needed to achieve optimal designs at higher Reynolds numbers.

**Keywords** Generalized shape optimization · Topology optimization · Lattice Boltzmann method · Adjoint sensitivity analysis · Low Reynolds number flow

---

G. Pingen (✉)  
Mechanical and Aerospace Engineering,  
University of Colorado, Colorado Springs, CO 80933, USA  
e-mail: pingeng@eas.uccs.edu, gpingen@eas.uccs.edu

M. Waidmann  
Mathematics and Computer Science,  
Freie Universität Berlin, 14195 Berlin, Germany

A. Evgrafov  
Department of Mathematics,  
Technical University of Denmark,  
2800 Kgs. Lyngby, Denmark

K. Maute  
Aerospace Engineering, University of Colorado,  
Boulder, CO 80309, USA

## 1 Introduction

The goal of this study is to investigate approaches to improve the performance of computational optimization methods for the design of incompressible fluidic systems with complex geometries, ranging in physical dimensions from Micro-Electro-Mechanical Systems (MEMS) to large scale external flows. Recently the authors have shown (Pingen et al. 2007a; Evgrafov et al. 2006) that the Lattice Boltzmann Method (LBM)

can be successfully employed for solving topology optimization problems in fluid mechanics and provide an interesting alternative to methods based on finite element Navier-Stokes solvers (see, e.g., Borrvall and Petersson 2003; Gersborg-Hansen et al. 2005; Aage et al. 2008). The LBM-based approach to flow topology optimization has been benchmarked against numerical examples previously solved by Borrvall and Petersson (2003) using a Navier-Stokes Finite Element Method (NS-FEM). Our numerical studies have not revealed any distinct advantages or disadvantages of the LBM scheme over the NS-FEM approach. In both cases, the layout of the flow domain is described by a material distribution approach relaxed via porous material models.

However, we have observed that both the LBM and NS-FEM optimization schemes suffer from a slow convergence of the optimization process and robustness issues at larger Reynolds numbers. While the general layout is obtained with a low number of optimization steps, finding the final shape is typically a slow process. A possible cause for the slow convergence is the “local” nature and large number of design variables in the “on-off” boundary representation of the traditional material distribution based approach. Here, a “local” design variable is one that affects only few (in the extreme case only one) elements or nodes in the discretized flow model. This local nature of the design variables drives the optimization of flow boundaries slowly, as most design variables only have a minimal effect on the objective.

At higher Reynolds numbers, the porous material in flow channels can lead to a premature onset of flow instabilities, thus leading to non-convergence of the flow solver, which in turn leads to non-convergence of the optimization process. Such a case is illustrated in Fig. 1 for a pipe-bend at  $RE = 400$ .

In the present work, we study whether we can improve convergence as well as versatility of topology op-

timization methods for fluidic systems by employing a level-set method. Level-set functions were originally introduced by Osher and Sethian (1988) for flame propagation problems in multi-phase flows. The development of level-set functions for fluid interface representation has been reviewed in detail by Sethian and Smerenka (2003). In addition to being used for fluid–solid interface tracking in fluid dynamics, level-sets have also been applied to combustion, image enhancement, and computer vision (see, e.g., Sethian 1999; Sethian and Smerenka 2003). The primary idea behind the level-set method is to introduce a function  $\Phi(\mathbf{x}, t)$  and define the interface  $\Gamma$  between two material domains  $A$  and  $B$  (e.g. fluid and solid) by the ‘zero-level-set’ ( $\Phi(\mathbf{x}, t) = 0$ ):

$$\begin{cases} \Phi(\mathbf{x}, t) < 0 & \text{if } \mathbf{x} \in \Omega^{(A)}, \\ \Phi(\mathbf{x}, t) = 0 & \text{if } \mathbf{x} \in \partial\Omega = \Gamma, \\ \Phi(\mathbf{x}, t) > 0 & \text{if } \mathbf{x} \in \Omega^{(B)}, \end{cases} \quad (1)$$

Here,  $\Omega^{(A)}$  represents material domain  $A$ ,  $\Omega^{(B)}$  represents material domain  $B$ . The evolution of the level-set function  $\Phi$  in the context of optimization is traditionally governed by a set of Hamilton-Jacobi (HJ) Equations ( $\Phi_t + \mathcal{H}(\nabla_x \Phi) = 0$ ) (Osher and Sethian 1988). The optimization algorithm controls the velocity with which the zero-levelset is propagated. Alternatively to the HJ approach, a parametric approach can be applied, where the level-set function is discretized by Radial Basis Functions (RBFs) and the resulting parameters are directly treated as optimization variables. This parametric approach is used in the present work and will be discussed in detail in Section 2.

Considering general PDE problems (e.g. for fluid or structural problems) the level-set function  $\Phi$  can be utilized to represent boundaries and has been applied for both shape and topology optimization (e.g. Sethian and Wiegemann 2000, Wang et al. 2003, Allaire et al. 2004; 2005, Burger and Osher 2005, Wang and Wang 2005, and Mohammadi and Pironneau 2008). Traditionally, body-fitted meshes coupled with a boundary parameterization through, e.g., splines (Fig. 2a), are used for shape optimization problems. Fixed meshes coupled with material distribution based geometry representation (Fig. 2c) are most commonly used for topology optimization. The boundaries defined through a level-set representation (Fig. 2b) can be mapped into the PDE solver via both body-fitted and fixed meshes. The boundaries can be represented explicitly via body-fitted meshes in combination with remeshing or mesh adaptation. Alternatively, the boundaries can be represented on fixed meshes via the material distribution approach or alternative immersed boundary methods. For the material distribution approach, the global level-set

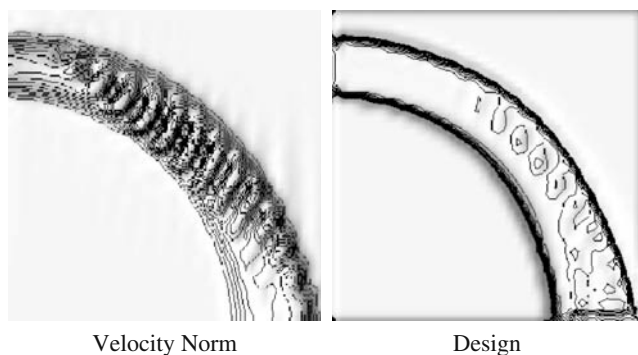
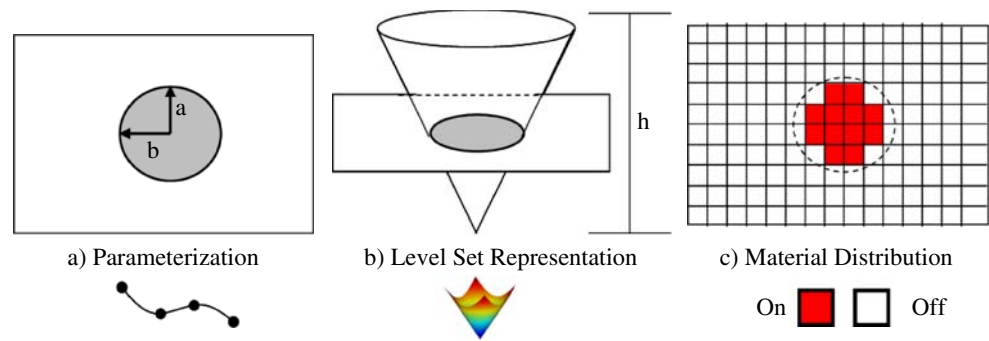


**Fig. 1** Design for a pipe bend at  $RE = 400$  on a  $50 \times 50$  lattice after 13 iterations

**Fig. 2** Illustration of flow boundary representations including the use of a 3D level-set function for a 2D boundary (a–c)



function (non-local design variables) is thus mapped into local densities/inverse porosities of a so-called Ersatz material.

As the level-set boundary representation decouples the material description from the discretization of the underlying partial differential equations, the same level-set model can be applied to distinctly different numerical schemes. Here, we study the performance of our parametric level-set model for the lattice Boltzmann method. The smooth level-set geometry can be represented in the LBM either through the use of a porosity model (Spaid and Phelan 1997), leading to a material distribution like topology optimization framework, or through the use of the interpolation bounce-back boundary condition (see Bouzidi et al. 2001), resulting in a generalized shape optimization scheme. In this work, the material distribution approach is studied in a framework initially implemented for fluidic topology optimization by the authors (Waidmann 2007; Pinggen et al. 2007b).

Possible advantages of using a level-set description of the fluid–solid interface rather than a traditional element-wise material distribution are the non-local impact of the design variables, the decoupling of the material description from the flow field discretization similar to the geometry projection method for shape optimization by Norato et al. (2004), and smooth design boundaries throughout the optimization process. The decoupling of the material description from the flow field discretization also provides flexibility in the resolution of the boundary geometry and the number of design variables used. Further, the smooth boundaries obtained with a level-set approach are expected to be of benefit for higher Reynolds number flow optimization, where non-smooth boundaries may cause the premature onset of unsteady flow as illustrated in Fig. 1.

For structural optimization, Sethian and Wiegemann (2000), Allaire et al. (2004, 2005), and Wang et al. (2003) have applied the HJ-level-set method to shape and topology optimization. The evolving contour of the structure during the optimization process is described by using a fixed Eulerian mesh and immersed boundary

techniques. Xia et al. (2006) further introduced a semi-Lagrange scheme in order to improve the efficiency of the HJ-level-set method during the optimization process. Wang and Wang (2005), Wei and Wang (2006), and Luo et al. (2008) used RBFs to discretize the classical HJ-level-set function and thus transform the original time dependent initial value problem into an interpolation problem (parametric level-set method). de Ruiter and van Keulen (2004) developed a parametric level-set method that does not involve the solution of the HJ-equation and applied it to structural topology optimization problems.

For fluid optimization with level-sets, only limited work has been done thus far. Cunha (2004) used parametric level-sets for shape optimization, finding shapes that re-produce a given velocity field for a stationary, viscous, incompressible fluid, using both Stokes and Navier-Stokes flow models. This approach has been applied by Terrel and Long (2006) to fluidic topology optimization problems to improve the Boolean “0-1” nature of the optimal solution for minimum-dispersion problems. In their work, Terrel and Long have used a simulated annealing optimization strategy. Waidmann (2007) and Pinggen et al. (2007b) combined a parametric level-set method with both a hydrodynamic lattice Boltzmann method and an incompressible Navier-Stokes flow model to optimize the layout of 2D flow domains. This approach is adopted in the present study. Duan et al. (2008) applied a slightly modified HJ-level-set method, a variational-level-set approach, to solve fluid shape optimization problems for Stokes and Navier-Stokes flows using gradient based methods. Mohammadi and Pironneau (2008) employed the HJ-level-set method for global shape optimization of aerodynamic design applications using a 2D potential flow model.

In the current work, we study the benefits and disadvantages of a parametric level-set approach for material distribution based topology optimization of fluids. In our level-set optimization framework the level-set function is essentially used to describe the material distribution with non-local parameters independent of

the fluid mesh and allows both merging and creation of obstacles. The flow is predicted by the hydrodynamic lattice Boltzmann method. First, the parametric level-set approach is introduced in Section 2, followed by a brief overview of topology optimization of fluids with the lattice Boltzmann method in Section 3. Finally, the parametric level-set method is applied to two topology optimization problems, a dual inlet, dual outlet flow channel design in Section 4.1 and a pipe bend for higher Reynolds number flows in Section 4.2.

## 2 Parametric level-set approach

In this study, a parametric level-set approach is used in combination with a gradient-based topology optimization framework for fluids. Our approach allows the generation and removal of new design features and utilizes the potential advantages of level-set methods (smooth boundaries, decoupling of material description from flow field discretization, and ‘non-local’ design variables). This approach is similar to the parametric level-set methods for structural material distribution based topology optimization introduced by Wang and Wang (2005), Wei and Wang (2006), Luo et al. (2008), and de Ruiter and van Keulen (2004), using radial basis functions  $\phi_j$  to parameterize the level-set function  $\Phi$ . Specifically, Wang and Wang (2005) and Wei and Wang (2006) have used multi-quadric and inverse multi-quadric basis functions, Luo et al. (2008) compactly supported Wendland basis functions, and de Ruiter and van Keulen (2004) Gaussian probability distribution functions as basis functions.

In the present approach, the following multi-quadric RBF is used:

$$\phi_j = s_j - \sqrt{(x - x_j)^2 + (y - y_j)^2 + c^2}. \tag{2}$$

Here the design variables  $s_j$  are initialized at every basis point  $j$  as illustrated in Fig. 3,  $c$  is a constant, and  $x, y$  are Cartesian coordinates spanning a given two dimensional design domain. The RBF (2) is a function of a single design variable that defines the height of the basis function (a cone). Multiple design variables can be used for each RBF to add additional flexibility, such as the cone angle, but are not studied in this work.

In general, the multi-quadric RBFs (2) are globally supported, meaning that each RBF  $\phi_j$  influences the level-set function  $\Phi$  throughout the entire design domain. By limiting the range of the design variables  $s_{\min} \leq s \leq s_{\max}$  and considering only the largest RBFs at each point to reduce the computational burden, the RBFs become locally supported. However, the support

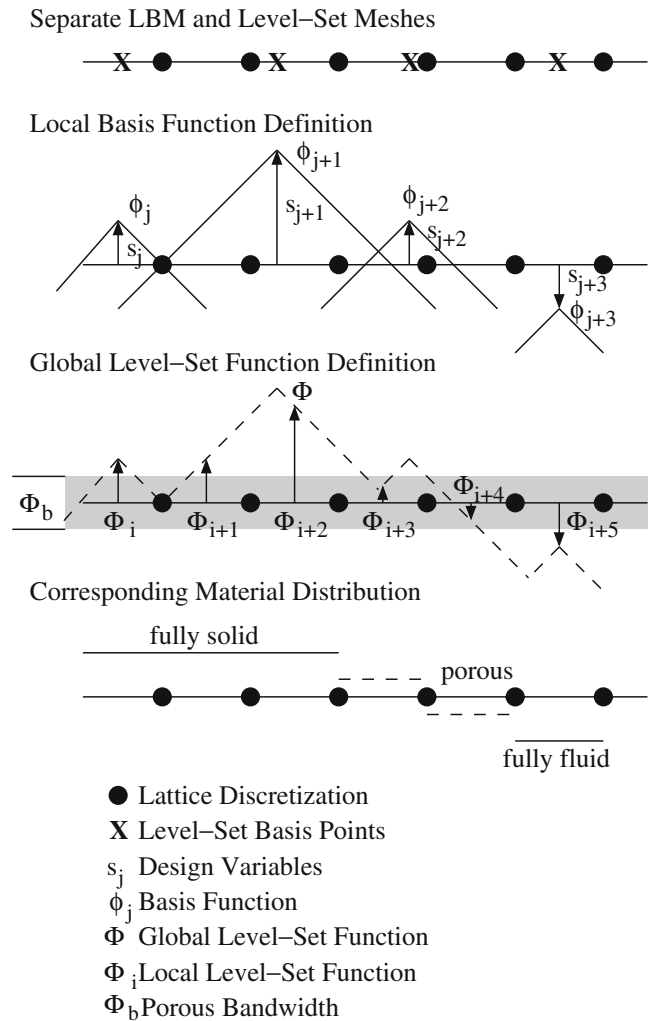


Fig. 3 Overview of the parametric level-set procedure

is adjustable and does not depend on the discretization of the fluid mesh.

The details of the mapping

$$s_j \mapsto p_i(\phi_j(s_j)), \tag{3}$$

from design variables  $s_j$  to a local material description through the use of basis functions  $\phi_j$  and the level-set function  $\Phi$  is illustrated in Fig. 3. Here, the local material description represents the inverse porosity  $p_i$  in the design domain (fluid ( $p_i = 0$ ), solid ( $p_i = 1$ )). Analogous to material distribution based approaches for flow problems, the computational domain is subdivided into  $n_{ele}$  elements. The level-set function  $\Phi$  is then evaluated at each element center by the maximum of all basis functions  $(\phi_j)_i$

$$\Phi(x_i, y_i) = \max_j (\phi_j)_i \quad \text{for } j = 1, \dots, n_\phi; i = 1, \dots, n_{ele} \tag{4}$$

where  $x_i, y_i$  denote the element centers and  $n_\phi$  is the total number of RBFs. Thus, the level-set function  $\Phi$  is the envelope of the RBF  $\phi$  distribution. However, the resulting level-set function  $\Phi$  is not differentiable and thus not suited for gradient based optimization. Alternatively, the maximum of all  $j$  locally evaluated RBFs  $(\phi_j)_i$  is approximated through the use of, for example, the  $m^{\text{th}}$ -norm of the local basis function values  $\phi_j$ ,

$$\Phi(x_i, y_i) = \left[ \sum_{j=1}^{n_\phi} [(\phi_j)_i + \Delta\phi]^m \right]^{\frac{1}{m}} - \Delta\phi. \tag{5}$$

both smoothing the resulting level-set function, and increasing the area of influence of each design variable. Since the  $m^{\text{th}}$ -norm approximation requires positive values of  $(\phi_j)_i$ , we use a shift  $\Delta\phi$  such that the minimal  $\phi_j$  value is always equal to or greater than zero. To reduce the error caused by the shift value,  $\Delta\phi$  is taken as the absolute value of the smallest  $\phi_j$  value occurring throughout the computational domain. Further, best results for the  $m^{\text{th}}$ -norm were obtained for  $70 \leq m \leq 90$  (Waidmann 2007) and a value of  $m = 90$  is used in the present work. This approach differs from the work by Wang and Wang (2005), Wei and Wang (2006), and de Ruiter and van Keulen (2004), who in essence use  $m = 1$  in (5) to determine  $\Phi$ .

In order to reduce the computational burden for determining the local level-set function values  $\Phi(x_i, y_i)$ , one can sample only over a subset of the basis functions  $\phi_j$ . For example, only the largest values of the basis functions  $\phi_j$  are considered to approximate the local maximum (5). In this study, the largest 10% of the local RBF values are considered. While this shortcut is not guaranteed to be differentiable, in our numerical experiments we have not observed any noticeable deterioration of the convergence of the optimization process when compared to using the differentiable approximation (5). The mapping from the basis functions  $\phi_j$  to the global level-set function  $\Phi$  for both an exact and approximated envelope of the level-set function are shown in Fig. 4.

Given the local level-set value  $\Phi(x_i, y_i)$ , a smoothed Heaviside function (shown in Fig. 5) is used to map the level-set function into a porosity value  $\Phi(x_i, y_i) \rightarrow p_i$  such that:

$$p_i(\Phi) = 1 - H(\Phi(x_i, y_i)) \tag{6}$$

where  $H$  is the smoothed Heaviside function,

$$H(\Phi) = \begin{cases} 0 & \text{if } \Phi(x_i, y_i) < -\chi, \\ h(\Phi) & \text{if } -\chi \leq \Phi(x_i, y_i) \leq \chi, \\ 1 & \text{if } \Phi(x_i, y_i) > \chi. \end{cases} \tag{7}$$

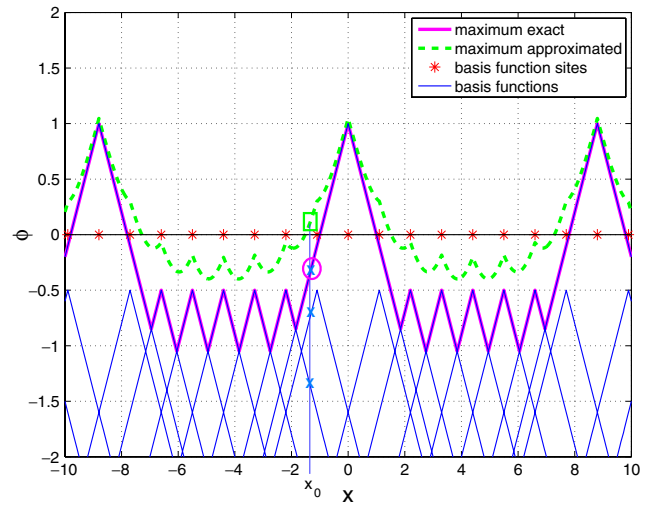


Fig. 4 Illustration of exact and approximated maximum in 1D

The corresponding derivatives of  $p$  with respect to the level-set function  $\Phi$  vanish when  $\Phi < -\chi$  and  $\Phi > \chi$ . The function  $h$  is defined as (see Osher and Fedkiw 2003; Sethian and Smerenka 2003),

$$h = \frac{1}{2} \left[ 1 + \frac{\Phi}{\chi} + \frac{1}{\pi} \sin\left(\frac{\pi\Phi}{\chi}\right) \right], \tag{8}$$

where the parameter  $\chi$  defines a band  $\Phi_b = 2\chi$  within which the Heaviside step function is smoothed. A wider band increases the smoothing of the Heaviside function but leads to a more fuzzy representation of the interface with an increase of intermediate porosity values. On the other hand, a narrow band yields a more crisp representation of the interface (closer to a “0-1” solution) but very few non-zero design sensitivities. This negatively affects the convergence of the gradient based optimization algorithms. In the extreme case, using the exact Heaviside function results in a non-differentiable mapping precluding the use of gradient-based mathematical programming algorithms.

The overall scheme described here leads to the following procedure when the design variables  $s_j$  are

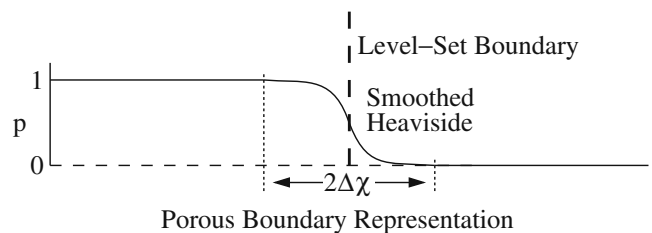


Fig. 5 Porous representation of the boundary

iteratively updated by the optimization algorithm. For a given level-set function  $\Phi$ , the resulting inverse porosities  $p_i$  are determined. Then, the governing equations and the adjoint sensitivity equations are solved to evaluate design criteria and their derivatives. Based on this information the optimization algorithm updates the vector of design variables  $s_j$ , which yields a modified level-set function  $\Phi$ . This process, illustrated in Fig. 6, is repeated until design convergence is obtained.

Compared to classical level-set approaches, where the optimization algorithm, the governing equations, and the level-set function are tightly coupled via the HJ-equation, the use of a parametric level-set approach allows employing mature mathematical programming schemes and can be easily integrated in existing topology optimization software. Furthermore, the parametric level-set approach introduced here allows the generation of new inclusions, made possible by the smoothing in the mapping (7–8) and by initializing level-set values within the smoothing bandwidth  $-\chi < \Phi_i < \chi$ . Thus, the present approach combines characteristics of topology optimization with those of shape optimization: generation of flow topologies/geometries and smooth boundaries. We refer to Fig. 12a for an example illustrating the generation of new design features.

### 2.1 Level-set sensitivity analysis

Based on (3) the derivative of the inverse porosities  $p_i$  with respect to the design variables  $s_j$  can be split into a product of three partial derivatives yielding,

$$\frac{\partial p_i}{\partial s_j} = \underbrace{\frac{\partial p_i}{\partial \Phi_i}}_c \cdot \underbrace{\frac{\partial \Phi_i}{\partial \phi_j}}_b \cdot \underbrace{\frac{\partial \phi_j}{\partial s_j}}_a \tag{9}$$

in component notation, with  $\Phi_i = \Phi(x_i, y_i)$  for clarity. The partial derivatives  $a$ . of the radial basis functions  $\phi$  (2) with respect to the design variables  $s_j$ ,  $b$ . of the level-set function  $\Phi_i$  (5) with respect to the basis func-

tions  $\phi_j$ , and  $c$ . of the inverse porosity  $p_i$  with respect to the level-set function  $\Phi_i$  are computed as follows:

$$\frac{\partial \phi_j}{\partial s_j} = 1, \tag{10}$$

$$\frac{\partial \Phi_i}{\partial \phi_j} = \left[ \frac{(\phi_j)_i + \Delta\phi}{\Phi_i + \Delta\phi} \right]^{(m-1)}, \tag{11}$$

$$\frac{\partial p_i}{\partial \Phi_i} = -\delta(\Phi_i) = \begin{cases} 0 & \text{if } \Phi_i < -\chi \\ -\frac{\partial h(\Phi_i)}{\partial \Phi_i} & \text{if } -\chi \leq \Phi_i \leq \chi \\ 0 & \text{if } \Phi_i > \chi \end{cases} \tag{12}$$

with

$$\frac{\partial h(\Phi_i)}{\partial \Phi_i} = \frac{1}{2\chi} \left[ 1 + \frac{1}{2\pi} \cos\left(\frac{\pi\Phi_i}{\chi}\right) \right]. \tag{13}$$

### 3 Topology optimization of fluids

The parametric level-set based topology optimization problem is cast into a generic nonlinear program of the following form:

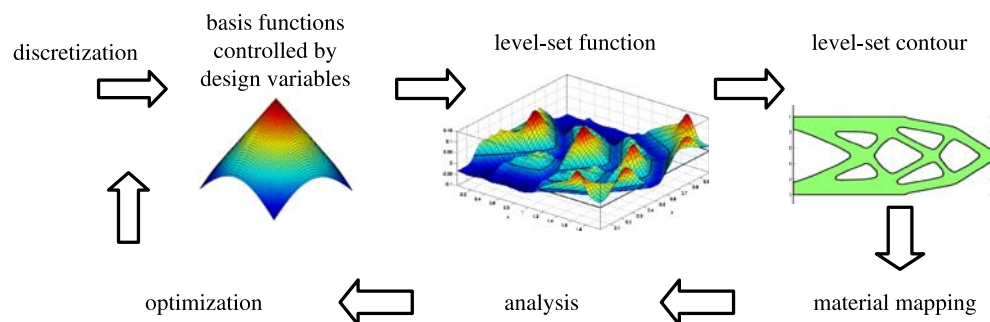
$$\begin{aligned} & \min_{\mathbf{s}} \mathcal{F}(\mathbf{s}, \mathbf{f}(\mathbf{s})), \\ & \text{s.t. } \begin{cases} \mathbf{s}, & \text{subject to design constraints,} \\ \mathbf{f}, & \text{solves the governing equations for a given } \mathbf{s}, \end{cases} \end{aligned} \tag{14}$$

where  $\mathcal{F}$  is a particular performance (objective) functional,  $\mathbf{s}$  is the vector of design variables, and  $\mathbf{f}$  is the corresponding state vector. In the current study, the loss of total pressure or pressure drop  $\mathcal{P}\mathcal{D}$  between fluid inlets and fluid outlets is considered as the objective  $\mathcal{F}$  and is defined as:

$$\mathcal{F} = \mathcal{P}\mathcal{D} = \int_{in} \left[ P + \frac{\rho}{2} |\mathbf{u}|^2 \right] - \int_{out} \left[ P + \frac{\rho}{2} |\mathbf{u}|^2 \right], \tag{15}$$

where  $P$  is the static pressure,  $\rho$  is the density, and  $\mathbf{u}$  is the flow velocity.

**Fig. 6** Overview of the present parametric level-set approach



The only constraint used in this study is a volume constraint, serving a dual purpose. First, the volume constraint limits the amount of fluid in the design domain, prescribing that at most a given fraction of the design domain,  $\gamma_F$ , is allowed to be occupied by fluid and the remainder must be solid. Second, the level-set approach to describe the material distribution does not lead to a “0-1” material distribution per se, and the volume constraint is utilized to encourage the desired “0-1” optimal solutions by reducing the amount of intermediate porosities in the design domain. The volume constraint is written as follows:

$$\gamma_F \leq \sum_i (1 - p_i^\kappa), \quad (16)$$

where  $\kappa$  is a polynomial shaping introduced to encourage “0 – 1” optimal solutions analogous to the porosity relation for the lattice Boltzmann method introduced in the following section. The properties of the shaping factor  $\kappa$  have been discussed in the authors’ recent work (Pingen et al. 2008). For high Reynolds number flows, it is important to implement the volume constraint as a penalty to the objective function in order to prevent flow blockage as discussed in Section 4.2.

For hydrodynamic problems, the flow is typically modeled by the Navier-Stokes equations which can either be directly discretized, commonly by finite volume or finite element methods, or approximated by the hydrodynamic lattice Boltzmann method as done in the present work. When solving the optimization problem (14), we solve for the design variables  $\mathbf{s}$  and the state variables  $\mathbf{f}$  are defined as implicit functions of the design variables. To permit a continuous transition from fluid to solid and vice versa, the governing hydrodynamic equations (Navier-Stokes or hydrodynamic lattice Boltzmann), are augmented. For topology optimization of fluids, a Brinkman penalization (Angot et al. 1999) is generally used to enforce the boundary conditions at the fluid–solid interface. This was done first by Borrvall and Petersson (2003), modifying the Stokes equation with a Brinkman term to model the flow through porous media (Brinkman 1947). Similarly, the authors (Pingen et al. 2007a) have applied the porosity model introduced by Spaid and Phelan (1997) for LBM topology optimization purposes. The resulting optimization problem (14) can then be solved with any large-scale gradient-based optimization algorithm. In this study, we use GCMMA by Svanberg (1995), a sequential convex approximation-based algorithm.

The following section introduces the lattice Boltzmann method and its application to topology optimization, including a brief discussion of the corresponding LBM sensitivity analysis.

### 3.1 Topology optimization with the lattice Boltzmann method

In recent years, the lattice Boltzmann method has become a popular alternative to conventional, Navier-Stokes based computational methods for a variety of problems in fluid dynamics (see, e.g., Yu et al. 2003, Succi 2001, and Chen and Doolen 1998). The hydrodynamic LBM approximates the Navier-Stokes equations and is based on the discretized Boltzmann equation, constituting a two step computational process:

*Collision:*

$$\tilde{f}_\alpha(\mathbf{x}_i, t) = f_\alpha(\mathbf{x}_i, t) - \frac{1}{\tau} [f_\alpha(\mathbf{x}_i, t) - f_\alpha^{eq}(\mathbf{x}_i, t)], \quad (17)$$

*Propagation:*

$$f_\alpha(\mathbf{x}_i + \delta t \mathbf{e}_\alpha, t + \delta t) = \tilde{f}_\alpha(\mathbf{x}_i, t). \quad (18)$$

In (17) and (18),  $\mathbf{e}_\alpha$  is the velocity vector,  $f_\alpha$  is the distribution function associated with the corresponding velocity  $\mathbf{e}_\alpha$ ,  $\mathbf{x}_i$  represents the location in physical space,  $\mathbf{e}_\alpha \delta t$  is the lattice spacing,  $\delta t$  is the time step, and  $\tau = \lambda / \delta t$  is the dimensionless relaxation time. For the current study, the two-dimensional 9-velocity model, D2Q9, is used.

For low Mach number flow conditions, the equilibrium distribution function  $f_\alpha^{eq}$  in (17) can be derived by a Taylor series expansion of the Maxwell–Boltzmann equilibrium distribution:

$$f_\alpha^{eq} = w_\alpha \rho \left[ 1 + 3(\mathbf{e}_\alpha \cdot \mathbf{u}) + \frac{9}{2}(\mathbf{e}_\alpha \cdot \mathbf{u})^2 - \frac{3}{2}\mathbf{u}^2 \right], \quad (19)$$

where  $\rho$  represents the macroscopic density, the vector  $\mathbf{u}$  is the macroscopic velocity, and  $w_\alpha$  are lattice weights that depend on the lattice geometry. The macroscopic parameters, such as density, velocity, pressure, and viscosity are evaluated by taking statistical moments of the distribution function  $f$ .

The porosity model of Spaid and Phelan (1997) can be used to augment the LBM to solve the Brinkman equations for porous flow through a minor modification of the collision step (17). The macroscopic velocity is rescaled during the collision step (17) for all lattice nodes occupied by the porous medium. We observe (Pingen et al. 2008) that the rate of convergence of the optimization algorithms is rather sensitive to the way velocities are scaled, and we obtain good results with the following polynomial scaling:

$$\tilde{\mathbf{u}}(t, \mathbf{x}_i) = (1 - p(\Phi_i)^\kappa) \mathbf{u}(t, \mathbf{x}_i), \quad (20)$$

where  $p(\Phi_i)$  represents the inverse porosity in the domain and  $\tilde{\mathbf{u}}(t, \mathbf{x}_i)$  is substituted into the equilibrium

distribution function (19) instead of  $\mathbf{u}$ . This porosity model permits a smooth transformation from fluid sites ( $p(\Phi_i) = 0$ ) into solid sites ( $p(\Phi_i) = 1$ ) as needed for topology optimization. Best results were obtained for  $\kappa \simeq 3$  (Pingen et al. 2008).

In this study we consider only steady-state flow problems which are described by the solution of the following fixed-point problem:

$$\mathbf{R}(\mathbf{f}, p) = \mathbf{M}(\mathbf{f}, p) - \mathbf{f} = \mathbf{0}, \tag{21}$$

where  $\mathbf{R}$  denotes the residual vector. Here, the operator  $\mathbf{M}$  performs one collision (17) and one propagation (18) step, advancing the flow to the next time step.

The derivatives of the performance functional  $\mathcal{F}$  are computed analytically by the adjoint method, owing to the large number of design variables. The derivative of the objective function  $\mathcal{F}$  with respect to the design variables  $\mathbf{s}$  can be written as follows:

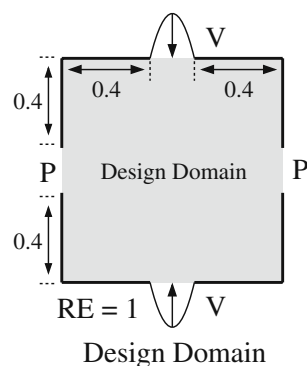
$$\frac{d\mathcal{F}}{ds_j} = \frac{\partial \mathcal{F}}{\partial s_j} - \left[ \left( \frac{\partial \mathbf{R}}{\partial \mathbf{f}} \right)^{-t} \frac{\partial \mathcal{F}}{\partial \mathbf{f}} \right]^t \frac{\partial \mathbf{R}}{\partial p_i} \frac{\partial p_i}{\partial s_j}. \tag{22}$$

where  $\mathbf{f}$  is the state vector at steady-state,  $\partial \mathbf{R} / \partial \mathbf{f}$  is the Jacobian of the LBM fixed-point problem (21), and  $\partial p_i / \partial s_j$  is the derivative of the level-set mapping from design variables  $s_j$  to material distribution  $p_i$  as introduced in Section 2.1.

### 4 Examples

To investigate the effectiveness of the parametric level-set approach for topology optimization of fluids, the approach is first compared to a standard material distribution based solution for a dual-inlet dual-outlet design problem shown in Fig. 7. Then the dependency of the ‘optimal’ design on algorithmic parameters and on the initial design is studied. Finally, in Section 4.2, the parametric level-set approach is applied to the optimal

**Fig. 7** Two inlet, two outlet optimization problem design domain



design of a pipe bend at intermediate Reynolds numbers ( $400 \leq RE \leq 1000$ ).

The level-set approach depends on four sets of adjustable parameters. These parameters are shown in the 1D level-set illustration in Fig. 8 and include the number of RBFs  $\phi_j$  and design variables  $s_j$  used, the maximum design variable step length for each iteration  $\Delta s_{\max}$ , the range of design variable values  $s_{\min} \leq s \leq s_{\max}$ , and the bandwidth  $\Phi_b = 2\chi$  for which the level-set function is mapped into the LBM inverse porosities  $p_i$ .

Initially these parameters were chosen analogous to the work by Waidmann (2007): The RBFs  $\phi_j$  can vary between  $-5 \lesssim \phi_j \lesssim 5$  by limiting the design variables:  $s^{\min} = -5 \leq s_j \leq 5 = s^{\max}$  (chosen rather arbitrarily). Analogous to Osher and Fedkiw (2003) the level-set bandwidth  $\Phi_b = 2\chi$  was chosen as  $\Phi_b = 1.5$ , leading to an inverse permeability increase from  $p = 0$  at  $\Phi = -0.75$  to  $p = 1$  at  $\Phi = 0.75$ . Our experience is that this range results in a relatively clear object boundary while providing sufficiently strong sensitivities as discussed in Section 2.1. Finally, the optimizer step length  $\Delta s_{\max}$  was set as  $\Delta s_{\max} = 0.005(s_{\max} - s_{\min})$  which is equal to 0.05 for the previously defined design variable bounds. This step length is equivalent to the optimizer step length used for material distribution based topology optimization in the authors’ previous studies (Evgrafov et al. 2006; Pingen et al. 2007a).

It should be noted that the presented results are an introductory study to understand and study the usefulness of the parametric level-set approach for fluids and the results were obtained with a MATLAB implementation of the level-set model and the LBM solver.

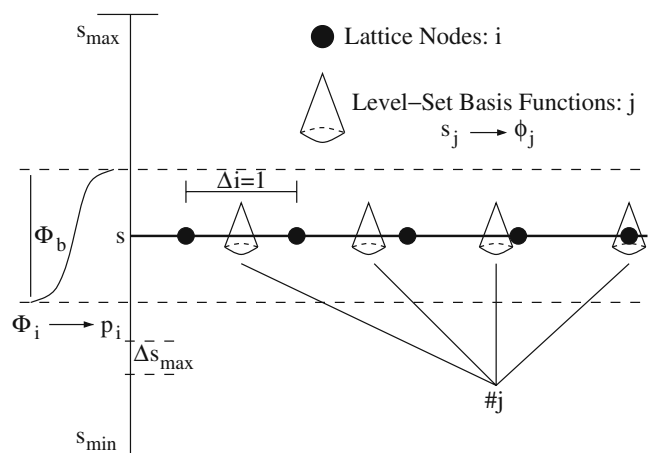


**Fig. 8** Illustration of the user-defined parameters in the level-set setup

4.1 Level-set validation

To demonstrate the viability of the parametric level-set method as an alternative to the traditional material distribution based scheme for flow problems, the two inlet, two outlet example shown in Fig. 7 is used. The design domain has two inlets (top and bottom) with prescribed velocities and two optional outlets (left and right) with prescribed pressure. The objective is to minimize the total pressure drop across the domain for a given maximum fluid volume of  $\gamma_F = 50\%$  at  $RE = 1$  with respect to the inlet width.

First, in Fig. 9 the results for the parametric level-set approach with the lattice Boltzmann method are compared with the traditional material distribution approach using the same number of design variables  $s_j$  on a  $41 \times 41$  mesh. The results have a similar topology after 100 iterations, at which point the material distribution approach is converged to its final solution. The LS approach appears to have converged as well, but suddenly develops a new local minima between iterations 500 to 600, resulting in an almost 50% improvement of the objective value as shown in Fig. 9c. This ability of the LS approach to improve the square symmetric (horizontal and vertical symmetry) design to an improved optimal solution of lower symmetry has been observed throughout this study and is attributed to the non-local nature of the design variables. However, the LS results are problem and parameter specific in that the LS approach leads to three different optimal solutions: square symmetry, horizontal symmetry, and diagonal symmetry depending on different parameter settings and initial designs as shown in Sections 4.1.1 and 4.1.2. The local nature of the design variables for the material distribution approach leads to a much stronger local minima, preventing optimal solutions of lower symmetry from the initial conditions. To overcome the local minima of a square symmetric solution for the material distribution approach, we have randomly perturbed the initial design variables by up to 10% of the design variable range  $s_{max} - s_{min}$ , however, without success. Finally, the porosity distribution plots in Fig. 9 show that both approaches (LS and material distribution) lead to “0-1” optimal solutions with slightly more intermediate porosities occurring along the boundary for the LS approach. These added intermediate porosities in the LS approach are due to the fuzziness introduced by the level-set bandwidth  $\Phi_b$ .

The convergence of the optimization problem for the LS and material distribution approaches is difficult to compare. First, both approaches lead to topologically different solutions. While the LS approach requires significantly more iterations to obtain a converged final

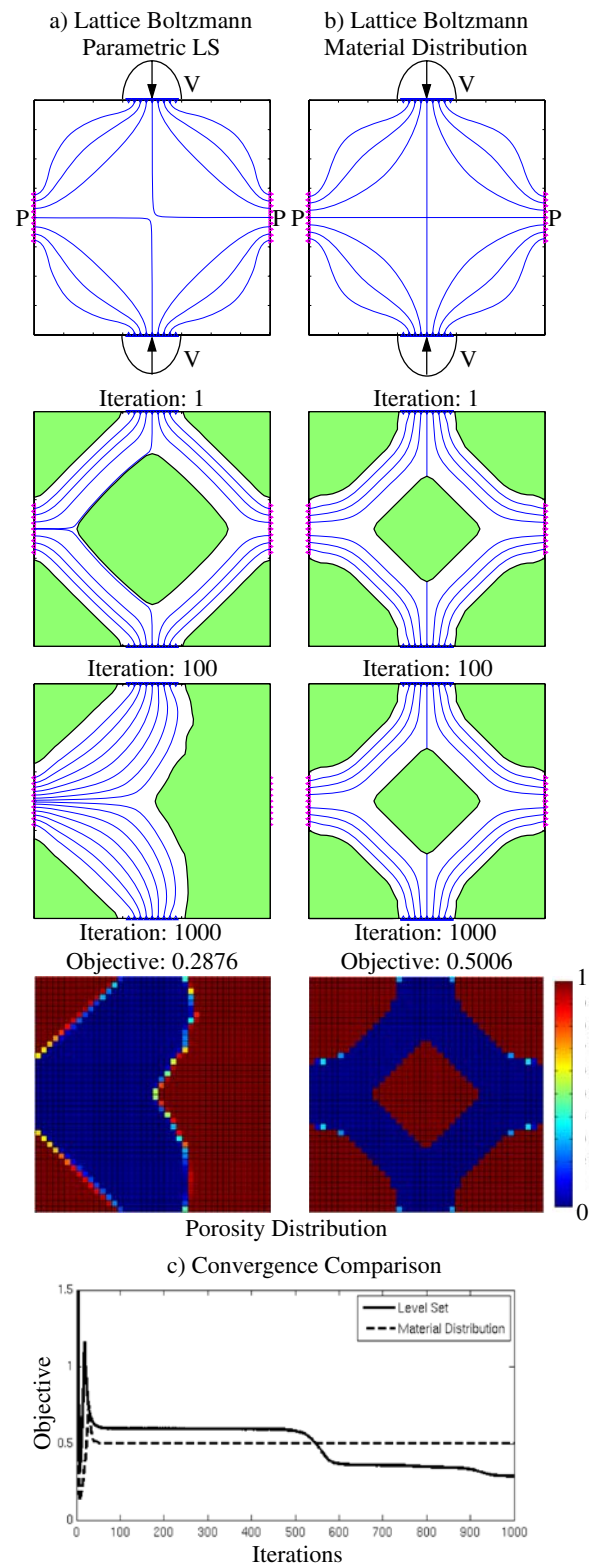


**Fig. 9** Comparison of boundary contour plots, porosity distribution, and design convergence for parametric level-set and traditional material distribution for the LBM flow solver (a–c)

result, the resulting design is significantly improved. Second, the objective value for the LS approach shows a more pronounced oscillatory behavior than the one for the material distribution approach. This is illustrated in Fig. 10, plotting the objective value of the final 100 iterations for LS and material distribution approaches. While the objective values differ in both methods, both oscillations are plotted on a y-axis spanning a change in objective of  $\Delta_{Obj} = 0.001$ . The rather large oscillations of the LS approach are caused by the strong nonlinearity introduced by the mapping (8) of the level set function onto the material distribution. These oscillations can be mitigated by a. increasing the bandwidth  $\Phi_b$ , which increases the blurring of the fluid–solid boundaries, and b. allowing for subcycling of the GCMMA algorithm, which increases the computational burden. Due to these reasons and in order to avoid premature termination of the optimization process, we do not apply a strict mathematical optimization criterion but stop the optimization process after a predefined large number of iterations (usually 1000).

In the introduction, we stated the expectation that the decoupling of material description and flow field discretization and the smooth design boundaries of the level-set approach would lead to larger, non-local sensitivities, which can better drive the optimization process towards an optimal solution. Our observation that the results do not show an improved convergence speed for the LS approach may be explained by the fact that the level-set function  $\Phi$  only actively impacts the design over a small bandwidth  $\Phi_b$  while the design variables in the material distribution based approach are always active. Thus, the level-set function  $\Phi$  only produces design sensitivities within the bandwidth  $\Phi_b$ . To analyze this effect further, the sensitivities for the design objective ( $d\mathcal{P}\mathcal{D}/ds_j$ ) for the material distribution based and parametric level-set based topology optimization process are compared at different optimization steps as shown in Fig. 11. The results show that the level-set

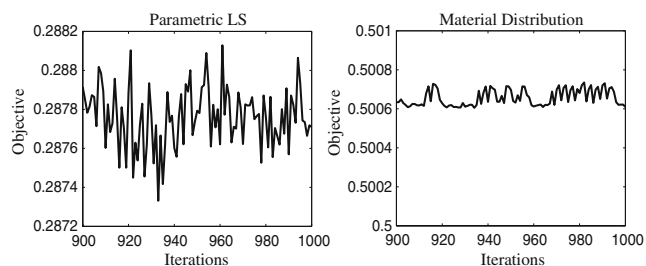


**Fig. 10** Comparison of convergence for parametric LS and material distribution based optimizations during the final 100 design iterations (Iterations 900–1000)

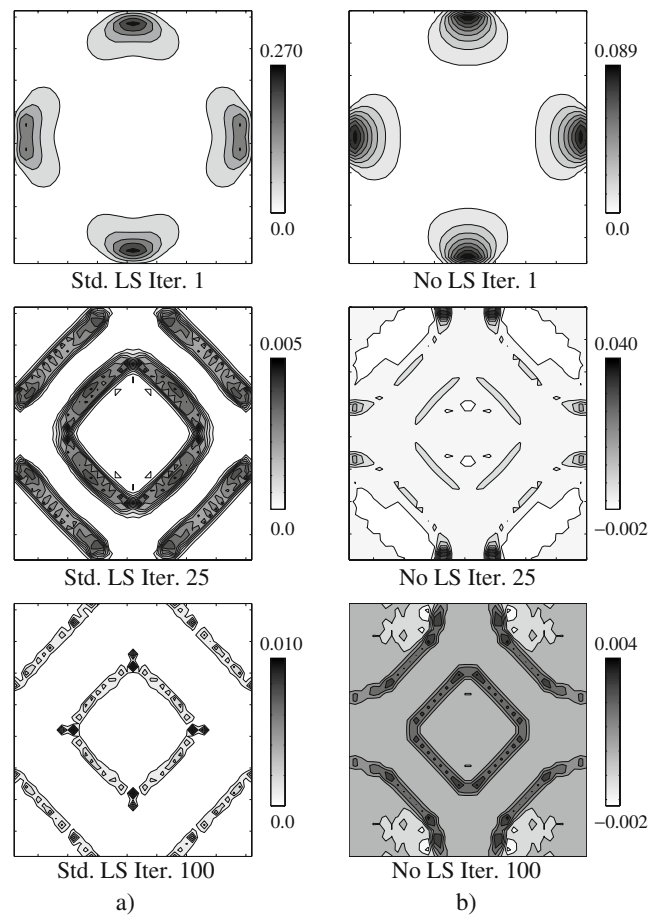


**Fig. 11** Comparison of design objective sensitivities for the LBM optimization process: **a** level-set, and **b** material distribution approach at three optimizer iterations (1, 25, 100)

sensitivities are larger for the initial flow state, but not for all iterations. While the parametric level-set method can in theory lead to non-local sensitivities, in practice the flow state is only sensitive to changes of design variables along the level-set front as shown for iterations 25 and 100 in Fig. 11. The material distribution approach also leads to sensitivities which are primarily located along the flow boundary, however, some sensitivities can be found outside the boundary region. Thus, as the optimization progresses, the level-set approach allows only a slow and step-wise movement of the existing boundary, limited by the optimizer step length  $\Delta s_{\max}$ , while changes beyond the boundary can occur in material distribution based optimization. The result suggests that the parameter level-set approach suffers from a similar limitation in advancing the level-set front as the traditional method based on the solution of the Hamilton-Jacobi equation where the CFL condition hampers the optimization process. In a detailed parameter study performed by Pinggen (2008), it is shown

that in particular the design variable step length  $\Delta s_{\max}$  has a significant impact on problem convergence while the level-set range  $s_{\min} \leq s \leq s_{\max}$  and the bandwidth  $\Phi_b = 2\chi$  have only a relatively small impact.

#### 4.1.1 Level-set initial design

To determine the impact of the initial design on the optimization results, in particular with respect to the ability to obtain non-symmetric solutions, 3 different initial conditions are studied as shown in Fig. 12. The uniform level-set initial condition (Fig. 12a) maps into a square symmetric (and approximately uniform) inverse porosity. Alternatively, we study two initial inverse porosity patterns with circular patches of solid material (Fig. 12b, c). The circular patterns are generated by initiating all but a few select design variables  $s_j$  at negative values. The first of the circular patterns (Fig. 12b) introduces several widely spaced cones with diagonal symmetry (“coarse-grained” circular pattern

with diagonal symmetry), while the second pattern uses 25 cones with square symmetry (“fine-grained” circular pattern with square symmetry).

It is observed that while the initial designs with square symmetry lead to a result that is horizontally symmetric as shown in Fig. 12a, c, the initial design with diagonal symmetry leads to a diagonally symmetric design as shown in Fig. 12b. This shows that for the current problem, the final solution is highly sensitive to the initial conditions and tends to adopt the symmetry of the initial designs. Incidentally, the objective values are almost equivalent for all designs in the present case. This study illustrates the strong effect that the choice of initial conditions can have on the final design solution and a test of multiple initial conditions is strongly recommended to identify locally optimal solutions. Additionally, Fig. 12 illustrates the potential of the applied parametric level-set approach to create new geometric features. While the optimization processes displayed in Fig. 12b and c require only the modification and merging of existing features, the optimization in

**Fig. 12** Comparison of level-set functions for different initial designs: **a** square symmetric (and approximately uniform), **b** “coarse-grained” circular pattern with diagonal symmetry, and **c** “fine-grained” circular pattern with square symmetry

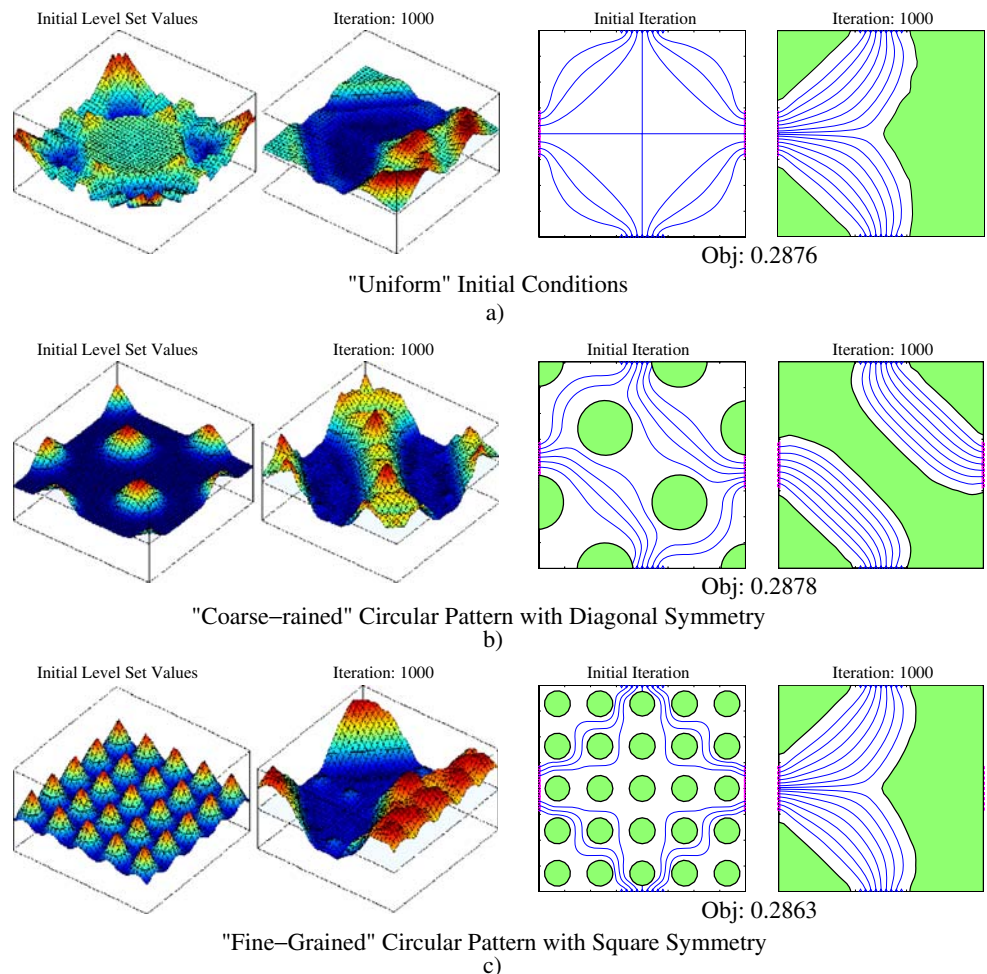
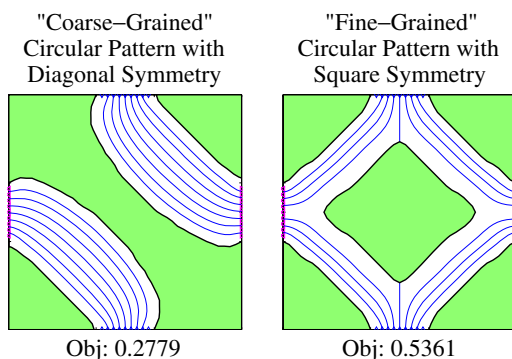


Fig. 12a includes the generation of several geometric features between the initial and final design states.

Figure 13 shows the effect of initiating the traditional material distribution based optimization approach with the “coarse-grained” circular pattern with diagonal symmetry initial design and the “fine-grained” circular pattern with square symmetry, respectively. The results show that using the diagonal circular pattern leads to a design analogous to the LS design in Fig. 12b, while the square circular pattern initial condition converges to a local-minimum with square symmetry.

#### 4.1.2 Number of level-set basis functions

One of the key features of the parametric level-set approach for fluidic topology optimization is the decoupling of the material description from the flow field discretization. Thus far, using a  $41 \times 41$  LBM mesh and a  $41 \times 41$  mesh of RBFs  $\phi_j$ , this decoupling has not been explicitly utilized. In this section, the effect of reducing the number of RBFs  $\phi_j$  and the corresponding design variables  $s_j$ , while maintaining a constant  $41 \times 41$  LBM mesh for the flow analysis, is studied. Figure 14 shows designs for  $41 \times 41$ ,  $37 \times 37$ ,  $33 \times 33$ ,  $29 \times 29$ ,  $25 \times 25$ ,  $21 \times 21$ ,  $17 \times 17$ ,  $13 \times 13$ , and  $9 \times 9$  RBFs  $\phi_j$ . The primary importance of this study is the observation that only the smallest set of radial basis functions  $\phi_j$  on a  $9 \times 9$  mesh shows signs of not being able to generate sufficiently refined boundaries. Thus, the ability to reduce the number of design variables while obtaining comparable optimal designs is promising for the studied problem. While the reduction of the number of design variables did not lead to improved optimizer convergence with the GCMMA, a reduced number of design variables enables the use of alternative and specialized optimization algorithms.



**Fig. 13** Material distribution results using an initial design of a coarse-grained circular pattern with diagonal symmetry and a fine-grained circular pattern with square symmetry

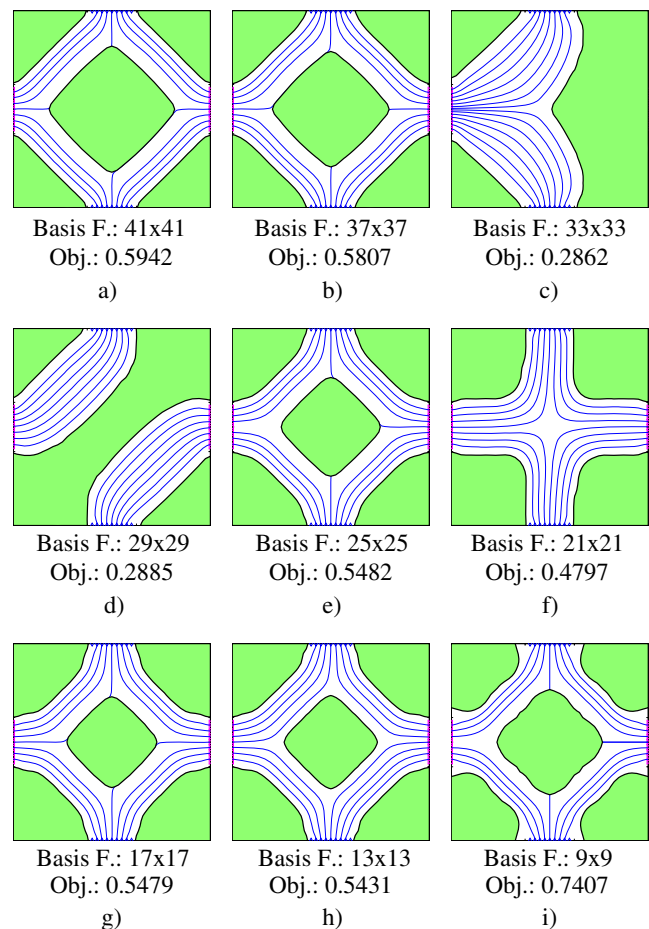


**Fig. 14** Comparison of optimal designs for a decreasing number of level-set basis functions  $\phi_j$  using 400 design iterations (a–i)

Finally, it is interesting to note that after 400 iterations, only two RBF meshes ( $33 \times 33$  and  $29 \times 29$ ), lead to optimal designs that are not square symmetric. A horizontally symmetric design is obtained for the  $33 \times 33$  mesh and a diagonally symmetric design is obtained for the  $29 \times 29$  mesh, both with nearly identical objective values.

#### 4.2 High Reynolds number study

In the authors’ introductory work on fluidic topology optimization with the lattice Boltzmann method (Pingen et al. 2007a; Evgrafov et al. 2006) a basic pipe-bend problem introduced by Borrvall and Petersson (2003) was solved and is shown in Fig. 15. The objective for this problem is to minimize pressure drop between inlet and outlet, subject to a 25% fluid volume constraint. It was shown that the curvature of the pipe bend increases for larger Reynolds numbers as shown in Fig. 16 due to competing physical effects: momentum loss due to shear stress and turning of the

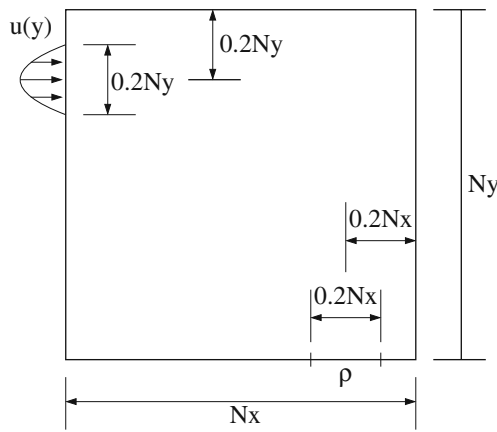


**Fig. 15** Pipe bend design domain with inlet and outlet conditions (Pingen et al. 2007a)

flow. These previous studies were limited to flows with  $RE \leq 100$ . For  $RE > 100$  designs with unsteady flows were generated, preventing the optimization algorithm to converge. However, unsteady flow is generally not expected until Reynolds numbers of  $RE \approx 1000$  for pipe bends. This flow unsteadiness was triggered by areas of intermediate porosity appearing within the flow channel throughout the optimization. The study of higher Reynolds number pipe-bends in this work was motivated by the smooth boundaries obtained with the level-set approach and the inherent restriction of areas with intermediate densities to the flow boundaries along the level-set front. The no-slip condition leads to slow velocities within the boundary region and thus no flow instabilities are expected for the pipe-bend within the considered Reynolds number range.

While studying the solution of optimal design problems for higher Reynolds number pipe bends with the parametric level-set approach, we observed that both the traditional material and level-set approaches suffered from triggering instationary flow solutions at intermediate design states. The improved smoothness of the boundaries and the confinement of porous areas of the level-set approach proved insufficient to avoid

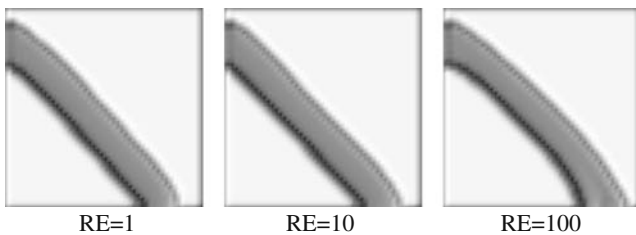


**Fig. 16** Pipe bend optimization results for Reynolds numbers between 0.1 and 100 (Pingen et al. 2007a)

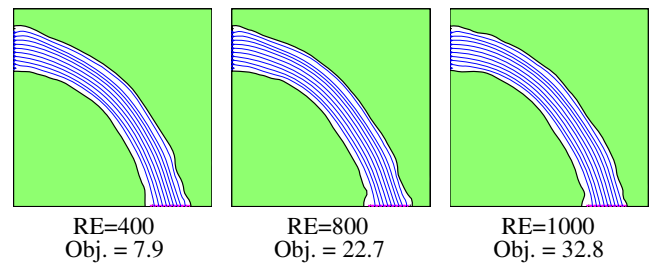


**Fig. 17** Level-set pipe bend optimization results for Reynolds numbers between 400 and 1000

this phenomenon. However, it was found that a key component to enable pipe-bend optimizations at higher Reynolds numbers is the gradual enforcement of the volume constraint (16) in order to prevent blockage of the flow channel. Here, a penalty based volume constraint defined as follows, is used,

$$\mathcal{P}_{\text{penalty}} = \sum_i (1 - p_i^k - \gamma_F),$$

and added to the pressure drop  $\mathcal{P}\mathcal{D}$  design objective,

$$\mathcal{F} = \mathcal{P}\mathcal{D} + \alpha \mathcal{P}_{\text{penalty}}. \tag{23}$$

This penalty formulation is enforced in the GCMMA algorithm by Svanberg (1995), and a penalty parameter  $\alpha = 100$  was used for the current problem.

Figures 17 and 18 show optimized designs for pipe-bends with Reynolds numbers ranging from 400 to 1000 using the parametric level-set formulation with uniform initialization and the traditional material distribution approach, respectively. The circular pattern initial conditions proved non-optimal for the pipe-bend optimization problem as they showed a tendency towards slowly converging multi-channel designs. The results in Figs. 17 and 18 show that the curvature of the pipe-bend continues to increase with increasing Reynolds number, as would be expected. Small differences between the designs, such as an overall improved boundary smoothness and small improvements in the objective value of the final designs, advocate the level-set approach.

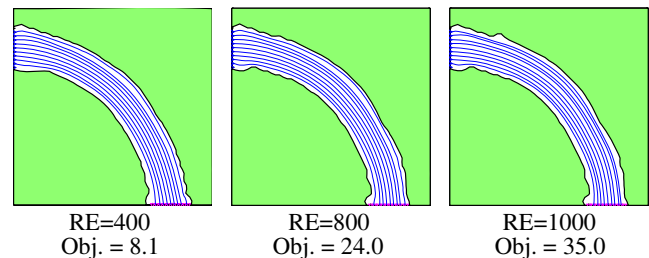


**Fig. 18** Traditional material-distribution pipe bend optimization results for Reynolds numbers between 400 and 1000

However, these differences are small and depend on specific level-set parameter settings and initialization. General conclusion cannot be drawn from these results. The optimal design of pipe-bends at even higher Reynolds numbers is currently not feasible due to the unsteady nature of those flows and the limitation of the current sensitivity analysis to steady-state flows.

## 5 Conclusions

We have studied a parametric level-set approach for flow topology optimization predicting the flow with a hydrodynamic lattice Boltzmann method. Following an Ersatz material approach, the level-set function is mapped into a material distribution. In the LBM analysis, the boundary conditions along the fluid–solid interface are enforced by a Brinkman approach using a porosity model. This study was motivated by a slow convergence of the optimization process and premature onset of instationary flows for higher Reynolds number flow problems.

The parametric level-set approach allows for decoupling of material description and flow field discretization, smooth design boundaries, and overall added versatility by linking design variables to local material properties through the use of a level-set function. The parametric level-set approach leads to similar optimal designs when compared to the traditional approach based on an element-wise discretization of the material distribution. Our numerical studies suggest that the parametric level-set mapping can be used to effectively reduce the number of design variables while maintaining similar optimized designs. However, our numerical experiments do not indicate that the level-set approach alleviates the problem of slow convergence of the optimization process.

While the parametric level-set approach can be applied to the solution of higher Reynolds number flow optimization problems, it has been shown that the key component for the solution of such problems is a gradual enforcing of the fluid volume constraint. Using a penalty formulation for the fluidic topology optimization framework has enabled an increase of the solvable flow regime from  $RE=100$  to  $RE=1000$  for the 2D pipe-bend. In the vicinity of  $RE=1000$ , the flow in the pipe-bend becomes unsteady and optimization is infeasible with the current steady-state flow model. Whether the potential improvement in boundary smoothness corresponding to the level-set representation leads to advantages remains to be seen for problems where the Reynolds number is further increased such that boundary layer effects become more significant. How-

ever, it should be noted at this point that the level-set function is mapped into a material distribution, resulting in a porous boundary layer, which possibly negates some of the benefits of the smooth level-set boundaries. Alternatively, the level-set function can be mapped into a direct boundary description such as the LBM interpolation boundary condition. This can potentially lead to a geometric topology optimization framework, merging benefits from shape optimization (exact/improved boundary representation) and topology optimization (generation of new topologies) into a single optimization tool, a topic that is currently being explored by the authors.

**Acknowledgements** The authors acknowledge the support of the National Science Foundation under grant DMI-0348759. The opinions and conclusions presented in this study are those of the authors and do not necessarily reflect the views of the sponsoring organization.

## References

- Aage N, Poulsen TH, Gersborg-Hansen A, Sigmund O (2008) Topology optimization of large scale stokes flow problems. *Struct Multidiscipl Optim* 35(2):175–180
- Allaire G, Jouve F, Toader AM (2004) Structural optimization using sensitivity analysis and a level-set method. *J Comput Phys* 194:363–393
- Allaire G, Jouve F, Toader AM (2005) Structural optimization using topological and shape sensitivity via a level set method. *Control Cybern* 34(1):59–80
- Angot P, Bruneau CH, Fabrie P (1999) A penalization method to take into account obstacles in viscous flows. *Numer Math* 81:497–520
- Borrvall T, Petersson J (2003) Topology optimization of fluids in stokes flow. *Int J Numer Methods Fluids* 41(1):77–107
- Bouzidi M, Firdaouss M, Lallemand P (2001) Momentum transfer of a lattice Boltzmann fluid with boundaries. *Phys Fluids* 13(11):3452–3459
- Brinkman HC (1947) A calculation of the viscous force exerted by a flowing fluid on a dense swarm of particles. *Appl Sci Res Sect A* 1:27
- Burger M, Osher S (2005) A survey on level set methods for inverse problems and optimal design. *Eur J Appl Math* 16: 263–301
- Chen S, Doolen GD (1998) Lattice Boltzmann method for fluid flows. *Annu Rev Fluid Mech* 30:329–364
- Cunha AL (2004) A fully Eulerian method for shape optimization with applications to Navier-Stokes flows. Ph.D. thesis, Department of Civil and Environmental Engineering, Carnegie Mellon University, Pittsburgh
- de Ruiter MJ, van Keulen F (2004) Topology optimization using a topology description function. *Struct Multidiscipl Optim* 26:406–416
- Duan X, Ma Y, Zhang R (2008) Optimal shape control of fluid flow using variational level set method. *Phys Lett A* 372(9):1374–1379. doi:10.1016/j.physleta.2007.09.070
- Evgrafov A, Pingen G, Maute K (2006) Topology optimization of fluid problems by the lattice Boltzmann method. In: Bendsøe MP, Olhoff N, Sigmund O (eds) IUTAM

- symposium on topological design optimization of structures, machines and materials: status and perspectives. Springer, Dordrecht, pp 559–568
- Gersborg-Hansen A, Sigmund O, Haber R (2005) Topology optimization of channel flow problems. *Struct Multidiscipl Optim* 30(3):181–192
- Luo Z, Wang MY, Wang S, Wei P (2008) A level set-based parameterization method for structural shape and topology optimization. *Int J Numer Methods Eng* 76:1–26
- Mohammadi B, Pironneau O (2008) Theory and practice of optimal shape design. *Eur J Comput Mech* 17(1–2):13–30
- Norato J, Haber R, Tortorelli D, Bendsøe MP (2004) A geometry projection method for shape optimization. *Int J Numer Methods Eng* 60:2289–2312
- Osher S, Fedkiw R (2003) Level set methods and dynamic implicit surfaces. In: *Applied mathematical science*, vol 153. Springer, Berlin Heidelberg New York, ISBN 0-387-95482-1
- Osher S, Sethian JA (1988) Front propagating with curvature dependent speed: algorithms based on Hamilton-Jacobi formulations. *J Comput Phys* 78:12–49
- Pingen G (2008) Optimal design for fluidic systems: topology and shape optimization with the lattice Boltzmann method. Ph.D. thesis, University of Colorado at Boulder
- Pingen G, Evgrafov A, Maute K (2007a) Topology optimization of flow domains using the lattice Boltzmann method. *Struct Multidiscipl Optim* 34:507–524
- Pingen G, Waidmann M, Evgrafov A, Maute K (2007b) Parametric-level-set approach to topology optimization of fluids with the Navier-Stokes and lattice Boltzmann equations. In: *Proceedings of WCSMO*
- Pingen G, Evgrafov A, Maute K (2008) Parameter sensitivity analysis for the hydrodynamic lattice Boltzmann method with applications to design optimization. *Comput Fluids*. doi:10.1016/j.compfluid.2008.10.002
- Sethian JA (1999) Level set methods and fast marching methods, evolving interfaces in computational geometry, fluid mechanics, computer vision, and material science. In: *Cambridge monographs on applied and computational mathematics*, vol 3, 2nd edn. Cambridge University Press, Berkeley
- Sethian JA, Smerenka P (2003) Level set methods for fluid interfaces. *Annu Rev Fluid Mech* 35:341–372
- Sethian JA, Wiegmann A (2000) Structural boundary design via level set and immersed interface methods. *J Comput Phys* 163(2):489–528
- Spaid MAA, Phelan FR (1997) Lattice Boltzmann methods for modelling microscale flow in fibrous porous media. *Phys Fluids* 9(9):2468–2474
- Succi S (2001) The lattice Boltzmann equation: for fluid dynamics and beyond. In: *Numerical mathematics and scientific computation*. Oxford University Press, Oxford
- Svanberg K (1995) A globally convergent version of MMA without linesearch. In: Rozvany G, Olhoff N (eds) *First world congress of structural and multidisciplinary optimization*. Pergamon, Oxford, pp 9–16
- Terrel AR, Long KR (2006) Evaluation of level set topology optimization formulations for design of minimum-dispersion microfluidic devices. In: *NECIS Summer Proceedings 2006*, pp 158–167
- Waidmann M (2007) A pseudo-level-set method for topology optimization of flows based on Navier-Stokes and lattice Boltzmann solvers. Master's thesis, University of Colorado at Boulder, Colorado
- Wang MY, Wang S (2005) Parametric shape and topology optimization with radial basis functions. In: *IUTAM symposium on topological design optimization of structures, machines and materials*, pp 13–22
- Wang MY, Wang X, Guo D (2003) A level set method for structural topology optimization. *Comput Methods Appl Mech Eng* 192:227–246
- Wei P, Wang MY (2006) Parametric structural shape and topology optimization method with radial basis functions and level-set method. In: *Proceedings of IDETC/CIE 2006, ASME 2006 international design engineering technical conferences*
- Xia Q, Wang MY, Wang S, Chen S (2006) Semi-Lagrange method for level-set-based structural topology and shape optimization. In: *Structural and multidisciplinary optimization*, vol 31. Springer, Berlin Heidelberg New York, pp 419–429. doi:10.1007/s00158-005-0597-y
- Yu D, Mei R, Luo LS, Shyy W (2003) Viscous flow computations with the method of lattice Boltzmann equation. *Prog Aerosp Sci* 39:329–367